Comparison of dynamic stall on an airfoil undergoing sinusoidal and VAWT-shaped pitch motions

Comparison of dynamic stall on an airfoil undergoing sinusoidal and VAWT-shaped pitch motions

C E Brunner[1], J Kiefer[2] and M Hultmark[1]

[1] Department of Mechanical and Aerospace Engineering, Princeton University, Princeton, New Jersey, USA.
[2] Department of Wind Energy, Technical University of Denmark, Kgs. Lyngby, Denmark.

E-mail: hultmark@princeton.edu

Abstract. The aerodynamics of vertical axis wind turbines (VAWTs) are inherently unsteady because the blades experience large angle of attack variations throughout a full turbine revolution. At low tip speed ratios, this can lead to a phenomenon known as dynamic stall. To better characterise the unsteady aerodynamics and represent them in models and simulations, data from studies of individual static or pitching airfoils are often applied to VAWT blades. However, these studies often involve sinusoidally pitching airfoils, whereas the pitching motions experienced by VAWTs are more complex. Here, the pressures and forces on an airfoil undergoing VAWT-shaped pitch motions corresponding to various tip speed ratios are compared to those of a sinusoidally pitching airfoil in order to assess whether a sinusoidal motion represents a reasonable approximation of the motions of a VAWT blade. While the lift development induced by the sinusoidal motion yields good agreement with that induced by the VAWT-shaped motion at the higher tip speed ratios, notable discrepancies exist at the lower tip speed ratios, where the VAWT motion itself deviates more from the sinusoid. Comparison with sinusoidal motions at reduced frequencies corresponding to the upstroke or downstroke of the VAWT-shaped motion yield better agreement in terms of the angle of stall onset.

1. Introduction

Although horizontal axis wind turbines dominate the wind energy sector, vertical axis wind turbines (VAWTs) have some benefits that might make them better suited for specific applications. For example, they are agnostic to wind direction, which is beneficial for deployment in turbulent urban environments. A recent report investigated the potential of VAWTs for offshore deployment, noting that they have a lower center of mass and a more easily accessible drive train [1]. However, these offshore turbines would be much larger and therefore operate at much higher Reynolds numbers than those typically studied for use in urban environments.

Aside from the Reynolds number Re_D, the flow across a vertical axis wind turbine is characterised by the tip speed ratio λ and the turbine solidity σ, which are defined as follows [2]:

$$Re_D = \frac{U_\infty D}{\nu} \qquad \lambda = \frac{\omega D}{2U_\infty} \qquad \sigma = \frac{nc}{D} \tag{1}$$

Here, ν is the kinematic viscosity, U_∞ is the freestream velocity, D is the turbine diameter, ω is its angular velocity, c is the blade chord length, and n is the number of blades. Another relevant parameter is the pitch angle β between the blade chord and the rotational velocity

vector, which is typically, but not necessarily, $\beta = 0°$ for vertical axis wind turbines. To study the aerodynamics of these turbines, it is often simpler to consider an individual blade or airfoil section. The aerodynamics of an individual turbine blade are characterized by the Reynolds number based on the chord length Re_c, the reduced frequency k, the angle of attack α, the velocity ratio u_{rel}, and the aspect ratio AR:

$$Re_c = \frac{\overline{U_r}\, c}{\nu} \qquad k = \frac{\pi\, f\, c}{\overline{U_r}} \qquad u_{rel} = \frac{U_r}{U_\infty} \qquad AR = \frac{s}{c} \tag{2}$$

Here, U_r is the relative velocity seen by the blade, f is the pitching frequency of the airfoil, and s is the airfoil span. Since U_r changes throughout a rotation, Re_c and k are defined as averages based on the mean relative velocity $\overline{U_r}$ following [3]. The aspect ratio is often ignored in studies of VAWT aerodynamics, but the effects of aspect ratio on blade behaviour are well established for static airfoils and have been shown to apply similarly to pitching airfoils [4]. Due to the presence of wing tip vortices, the lift increases more slowly and stall occurs at higher angles of attack on blades with low aspect ratios.

VAWTs are not currently deployed at commercial scales, in part due to the complexity of their aerodynamic behaviour and associated structural issues. Because the axis of rotation of a VAWT is perpendicular to the incoming flow, its blades experience rapidly fluctuating inflow velocities. In the reference frame of a blade, the direction and magnitude of the inflow velocity are typically approximated as follows:

$$\alpha = tan^{-1}\left(\frac{(1-a)\, sin\theta}{(1-a)\, cos\theta + \lambda}\right) \qquad u_{rel} = \sqrt{(1-a)^2 + 2\,(1-a)\,\lambda\, sin\theta + \lambda^2} \tag{3}$$

Here, α is the angle of attack seen by the blade, θ is the azimuthal position of the blade, λ is the tip speed ratio of the turbine and u_{rel} is the inflow velocity to the blade, normalized by the freestream velocity. At $\theta = 0$, the blade is facing the freestream head on, such that $0 \leq \theta \leq \pi$ is the upstream half of the rotation, and $\pi \leq \theta \leq 2\pi$ is the downstream half. The induction factor accounts for the deceleration of the flow as it approaches the turbine. It is defined as $a = 1 - U_a/U_\infty$, where U_a is the flow velocity just upstream of the turbine, and therefore assumes values of $0 \leq a \leq 1$. [5] found that the induction factor generally assumes values of $0 \leq a \leq 0.35$ over the upstream half of the turbine, which is responsible for the majority of thrust, and $0 \leq a \leq 0.65$ over the downstream half of the turbine. The higher the induction factor, the more severe the fluctuations in angle of attack and inflow velocity experienced by an individual blade at a given tip speed ratio.

Viewed from the reference frame of the inflow velocity, the motion described above is equivalent to a blade that is simultaneously pitching and surging in a steady freestream. Pitching and surging airfoils have been widely studied. If the oscillations are small, such that the airfoil does not stall, the flow experiences only mild unsteady effects. The lift and moments on the blade are well approximated by thin airfoil theory [6, 7].

If the angle of attack fluctuations are large enough that the maximum angle of attack significantly exceeds the static stall angle of the airfoil, a phenomenon known as dynamic stall occurs [8, 9]. Dynamic stall leads to an overshoot in the lift force as the flow momentarily remains attached beyond the static stall angle, followed by drastic stall as a vortex forms on the suction side of the airfoil and convects downstream. This can lead to structural failure of the turbine over time [10]. Furthermore, accurate performance predictions require that the forces produced during dynamic stall are captured by VAWT models.

Analytical models of VAWTs typically require tabulated lift and drag coefficient data of the specific airfoil as input [11]. This data is obtained from either experiments or blade-scale numerical simulations. Turbine-scale numerical simulations also sometimes use tabulated airfoil

data in order to reduce computational costs [12]. Empirically derived dynamic stall models are typically applied to the data to correct for unsteady effects, e.g. [13, 14]. However, these models are relatively simplistic and do not account, for example, for Reynolds number effects.

Recent efforts have therefore attempted to better characterise dynamic stall on VAWT blades. Many of these studies focus on pitching and surging airfoils as an approximation of full VAWT blade aerodynamics [15, 16]. The parameters governing dynamic stall on an airfoil (equation 2) are related to the relevant VAWT parameters (equation 1) as follows:

$$k = \frac{c}{D} \qquad Re_c = \lambda \frac{c}{D} Re_D \tag{4}$$

Note that these relationships require that Re_c and k are defined in terms of the average velocity $\overline{U_r} = \omega R$, not the instantaneous velocity. Equation 4 reveals that the reduced frequency k is solely a function of the turbine geometry. Furthermore, equation 3 implies that lower tip speed ratios lead to larger fluctuations in the angle of attack and the inflow velocity. As such, dynamic stall is primarily expected to occur at low tip speed ratios because the blade is then more likely to exceed its static stall angle.

In previous studies, varying degrees of simplification have been applied to the original VAWT aerodynamics. Some studies consider an individual blade that is part of a single-blade or multiple-blade turbine, usually at Reynolds numbers considerably lower than expected for field conditions [17]. Studies at higher Reynolds numbers typically consider an individual airfoil that is pitching and heaving to reproduce a VAWT-shaped motion. This simplification ignores the Coriolis force acting on the blade, the effect of which was studied by [18]. It also ignores the curvature effect caused by the curvature in the streamlines of the flow experienced by a VAWT blade, which can lead to effective cambering of the airfoil [19]. The importance of this effect depends on $k = c/D$. Many studies also do not involve surging and instead focus on pitching. Lastly, the airfoil is often pitched sinusoidally instead of according to equation 1 due to the limitations of experimental equipment [15, 16].

Tsai and Colonius compared the aerodynamics of an airfoil undergoing sinusoidal and VAWT-shaped pitching up to a Reynolds number of $Re_c = 1500$ [18]. They found that the sinusoidal motion overestimates the lift force as a function of angle of attack on the upstroke due to the higher pitch rate compared to the VAWT-shaped motion. The lower the tip speed ratio, the larger the difference, since the VAWT-shaped motion deviates more from the sinusoid. However, the Reynolds number in this study is at least two orders of magnitude lower than that of full-scale VAWTs and the flow is therefore expected to remain fully laminar unlike the full-scale flow.

The present study builds on the work of Tsai and Colonius by comparing a sinusoidal pitching motion to a VAWT-shaped pitching motion at $Re_c \sim O(10^6)$. Under these conditions, the insights gained are relevant to full-scale Darrius-type VAWTs. We investigate the effect of tip speed ratio on the dynamic stall process and develop a more accurate way to use data from sinusoidally pitching airfoils for VAWT models and numerical simulations.

2. Methodology

2.1. Experimental setup

Reynolds numbers of $1.0 \times 10^6 \leq Re_c \leq 2.0 \times 10^6$ were achieved using the High Reynolds number Test Facility (HRTF) at Princeton University. The HRTF uses highly pressurized air (up to 220 atm) as the working fluid. As a result, the Reynolds number can be increased by increasing the density while leaving the velocity low. This allows for studies of unsteady aerodynamics at relatively high reduced frequencies and high Reynolds numbers, while keeping the convective timescale low, thereby allowing for sufficiently high temporal resolution of the unsteady effects. The HRTF has a round test section with a diameter of 0.5 m.

A NACA 0021 was used, as this airfoil has been studied in previous VAWT-related experiments, e.g. [20]. The airfoil has a chord length of 0.17 m, an aspect ratio of 1.5 and is equipped with end plates to reduce three-dimensional effects. Due to the thickness of the airfoil, the high Reynolds numbers and the low aspect ratio, the static stall angle is $\alpha_{ss} = 21.8°$ at $Re_c = 1.0 \times 10^6$ and $\alpha_{ss} = 22.4°$ at $Re_c = 2.0 \times 10^6$. Full-scale VAWTs typically have aspect ratios higher than the airfoil studied here, however without end plates. They are therefore not expected to perfectly follow two-dimensional airfoil behaviour. Instead, they presumably fall somewhere between two-dimensional airfoils and the model studied here, as far as three-dimensional effects are concerned.

The airfoil is equipped with 32 pressure taps distributed chordwise along the surfaces of the airfoil. The pressure taps are connected to pressure transducers housed inside the airfoil. This yielded tube lengths of < 0.25 m between taps and transducers in all cases. Given the relatively low pitching frequencies required to achieve dynamic effects, the lag in the pressure readings due to the tubing is assumed to be negligible. The pressure measurements were integrated to yield the resulting forces and moments on the airfoil. The measurements were phase-averaged over 148 cycles. No corrections were applied to the data. In [21] static data from this setup was corrected for blockage and aspect ratio and showed good agreement with previous studies of this airfoil. The reader is referred to [21] and [9] for more details on the experimental setup.

2.2. Pitch motions

Pitch motions corresponding to a sinusoidal shape as well as to several VAWT-shaped motions were tested. The angle time histories are shown in figure 1a). The VAWT-shaped motions were chosen such that the maximum angles of attack α_{max} were delayed by $0.175n$ radians with $n = \{1, 2, 3, 4\}$ compared to α_{max} of the sinusoid, while the minimum angle of attack α_{min} occurred $0.175n$ radians earlier. This leads to a slower upstroke and faster downstroke compared to the sinusoid. The VAWT-shaped pitch motions are therefore inherently asymmetric. They correspond to various tip speed ratios as specified by equation 3. The higher the tip speed ratio, the more closely the motion resembles a sinusoid. Equation 3 was used to determine the specific tip speed ratios corresponding to the motions studied here. For simplicity, the induction factor was assumed to be zero, which resulted in tip speed ratios of $\lambda = \{5.7, 2.8, 1.9, 1.4\}$. At induction factors of $a > 0$, the corresponding tip speed ratios would be slightly lower.

On a VAWT, varying the tip speed ratio will also lead to varying amplitudes of the angular pitch motion. Because the purpose of this study was not to compare various tip speed ratios with one another, but rather to evaluate whether the motion at a given tip

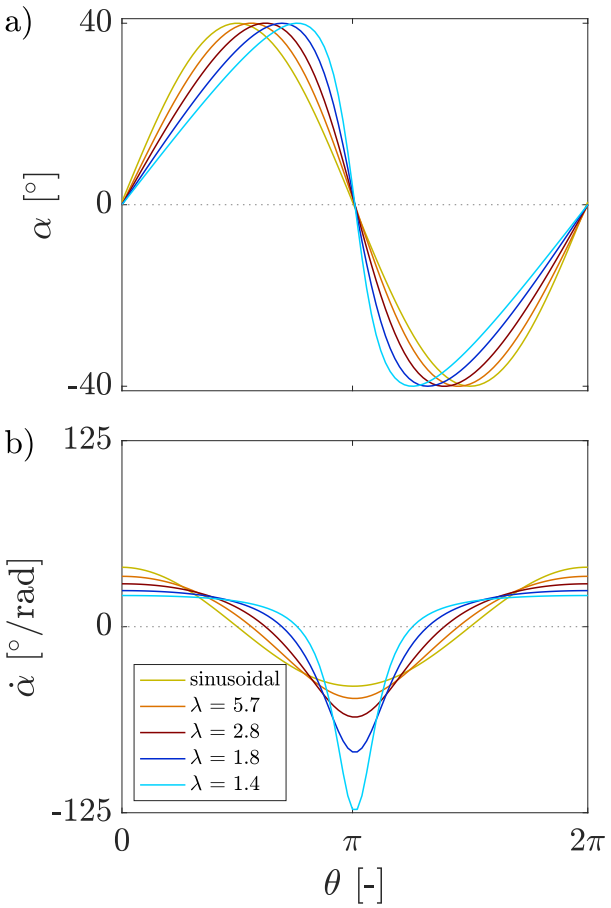

Figure 1. Angle of attack and pitch rate throughout a full turbine rotation.

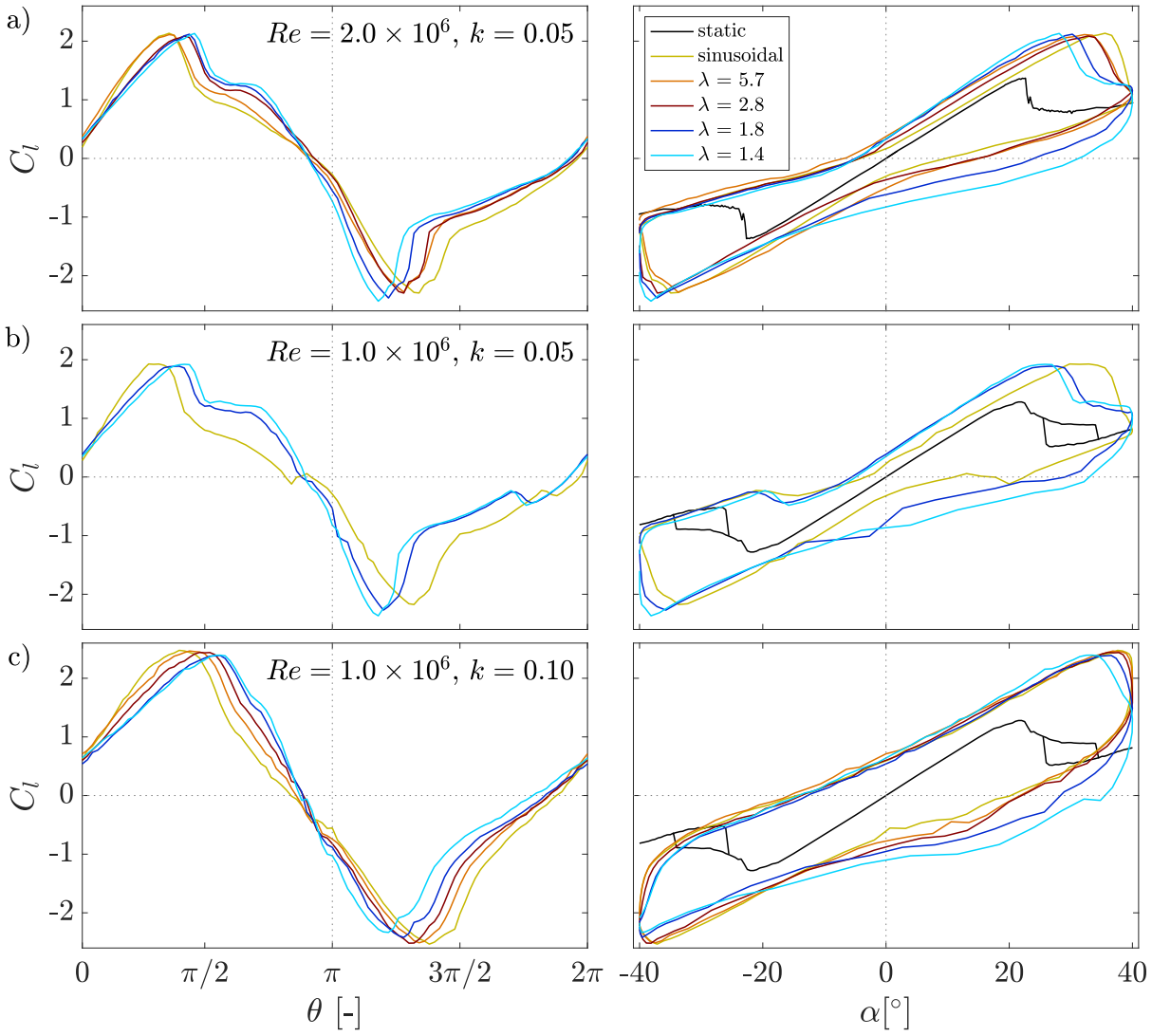

Figure 2. Lift coefficient as a function of azimuth θ and angle of attack α. Note that the data in the right and left panels are the same.

speed ratio can be approximated as sinusoidal, the amplitudes of motion were all normalised to $\hat{\alpha} = \pm 40°$ around a mean angle of attack of $\bar{\alpha} = 0°$. This was the largest amplitude that could be achieved with this experimental setup and therefore resulted in the most severe dynamic stall effects. The static stall angles of $\alpha_{ss} = 21.8°$ at $Re_c = 1.0 \times 10^6$ and $\alpha_{ss} = 22.4°$ at $Re_c = 2.0 \times 10^6$ were significantly exceeded in all cases. The high static stall angles are due to the relatively low aspect ratio of the airfoil used here. The corrections applied in [21] suggest that an angle of $\alpha = 40°$ in the present setup corresponds to an angle of $\alpha = 33.2°$ on an infinite aspect ratio airfoil. For reference, according to equation 3 the maximum amplitude achieved by a VAWT blade with an induction factor of $a = 0$ is $\hat{\alpha} = 10.1$ at $\lambda = 5.7$ and $\hat{\alpha} = 45.6$ at $\lambda = 1.4$. Higher induction factors lead to larger amplitudes. Details of the individual test cases are listed in table 2 in the appendix. The pitch rate is shown in figure 1b). It provides intuition for the key differences between the motions and their effects on the stall process.

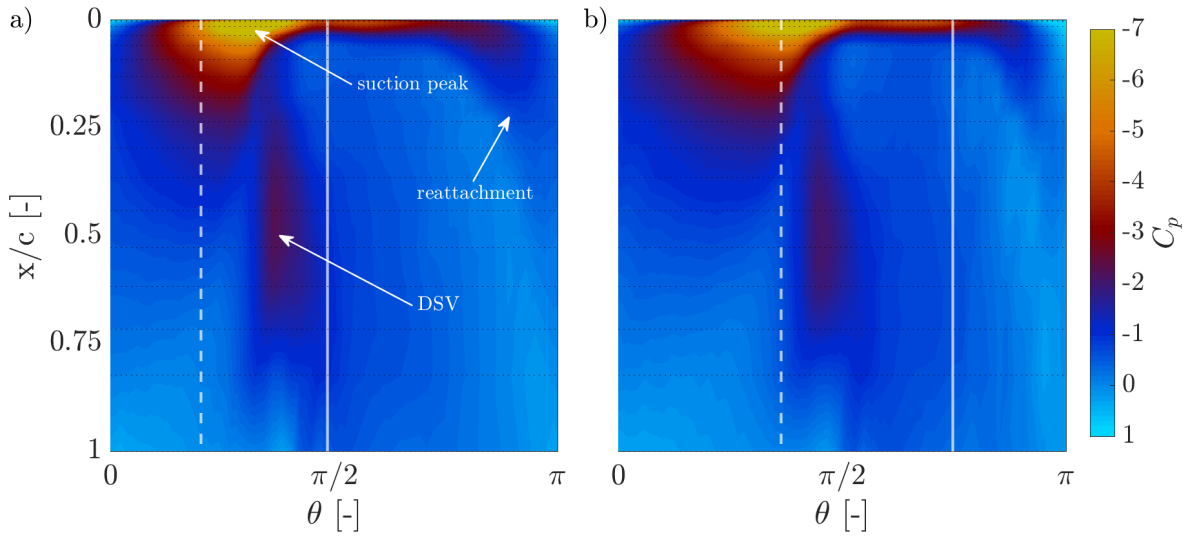

Figure 3. Top-side surface pressure distributions at $Re = 2.0 \times 10^6$, $k = 0.05$ of a sinusoidal pitching motion in a) and a VAWT-shaped motion with $\lambda = 1.4$ in b). Dashed lines indicate the time when the static stall angle is passed and solid lines mark $\alpha_{max} = +40°$. DSV is the dynamic stall vortex.

3. Results and discussion

3.1. Lift development

The lift coefficient C_l is not only one of the key parameters needed to model VAWTs, it also provides insight into the stall and reattachment processes. Figure 2 shows the development of C_l throughout a full turbine rotation, both as a function of azimuth θ, i.e. nondimensional time, and as a function of angle of attack α. At $\theta = 0$ and $\theta = 2\pi$ the angle of attack is $\alpha_{min} = -40°$. The azimuth at which α_{max} occurs varies with tip speed ratio. Under all conditions tested, the dynamic lift development deviates significantly from the static lift curve, even around $\alpha = 0$. The flow stays attached far beyond the static stall angles and generates significantly higher lift. Once stall has occurred, the flow does not reattach immediately, despite the declining angle of attack, which leads to large hysteresis loops in the left panel of figure 2.

While the lift of the sinusoidal motion is symmetric around $\alpha = 0$, the lift of the VAWT-motions becomes increasingly asymmetric as tip speed ratio decreases. The main discrepancies between the sinusoid and the VAWT-shaped motions are in the onset of stall as well as the reattachment during the accelerated downstroke. Because decreasing the tip speed ratio delays α_{max}, it also delays the maximum lift $C_{l,max}$. This leads to a momentary lift plateau after stall has occurred in figures 2a) and b). Plotted against α, stall on the upstroke seems to occur sooner at lower tip speed ratios. On the downstroke, the opposite occurs. The stall process is slightly delayed, leading to slightly lower $C_{l,min}$. Reattachment on the accelerated downstroke is increasingly delayed as tip speed ratio is decreased. This implies that the flow requires a certain amount of time to reattach, which is independent of the pitch rate.

Minor Reynolds number effects are visible when comparing panels a) and b) in figure 2. Stall occurs slightly earlier at the lower Reynolds number of $Re_c = 1.0 \times 10^6$. This is in agreement with the decrease in the static stall angle [21]. It indicates that the static stall angle plays an important role in dynamic stall. The transition to more gradual trailing-edge stall and reattachment hysteresis at the lower Re_c under static conditions does not seem to affect the dynamic stall process.

For the data shown in figure 2c) the reduced frequency was increased to $k = 0.10$, effectively

doubling the pitch rate compared to figure 2b). At this reduced frequency, the flow stays attached on the downstroke until α_{min} is reached, while on the upstroke it stays attached until α_{max} for the sinusoid and the higher tip speed ratios. At the lowest tip speed ratios of $\lambda = 1.8$ and $\lambda = 1.4$, stall occurs slightly ahead of α_{max} on the upstroke and slightly beyond α_{min} on the downstroke, effectively stalling when the angle is already increasing. The delay in the reattachment on the accelerated downstroke is more pronounced than at $k = 0.05$. This further suggests that the reattachment process is governed by a timescale independent of the pitch rate. On the upstroke, the agreement in the lift as a function of α is surprisingly good at $k = 0.10$.

3.2. Pressure distributions

The pressure distributions on the suction side of the airfoil elucidate the effect of tip speed ratio on the dynamic stall process. Figure 3 compares these pressure distributions over $0 \leq \theta \leq \pi$ for a sinusoid and a VAWT-shaped pitch motion with $\lambda = 1.4$, both data sets at $Re_c = 2.0 \times 10^6$ and $k = 0.05$. The region to the left of the solid line is the latter half of the upstroke, and the region to the right of it is the first half of the downstroke. The sinusoid in figure 3a) is symmetric, so that the upstroke and downstroke are equal in length. For $\lambda = 1.4$ in figure 3, the upstroke is decelerated and therefore significantly longer than the accelerated downstroke. The yellow regions indicate the maximum suction peaks, while the dark red regions at $x/c \approx 0.5$ mark the dynamic stall vortices convecting downstream [9]. Because the static stall angle is passed later in time at $\lambda = 1.4$, stall occurs slightly later in time. However, the time between the passing of α_{ss} and of α_{max} is longer as the airfoil is moving more slowly, so that stall occurs at a lower angle of attack.

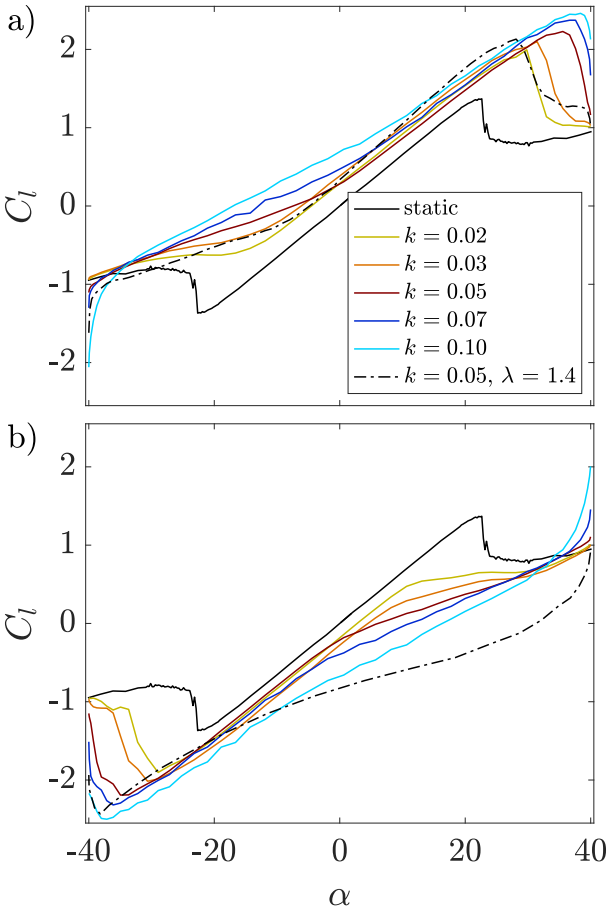

Figure 4. Lift coefficient development during the upstroke (a) and downstroke (b) for a range of reduced frequencies $0.02 \leq k \leq 0.10$ and $Re_c = 2.0 \times 10^6$. Unless otherwise noted, the motion is sinusoidal.

3.3. Tip speed ratio correction

The above observations reveal that the reduced frequency does not sufficiently characterise the dynamic stall process of airfoils undergoing differing pitch motions. This supports the findings of [22]. Because the pitch velocity varies significantly between the upstroke and the downstroke, the unsteadiness of the flow is more aptly described by two separate reduced frequencies, one corresponding to the upward pitch and the other to the downward pitch. Table 3.3 shows the effective reduced frequencies of the upstroke and downstroke at the tip speed ratios considered here. These are calculated using $k_{up/down} = k\pi/(\pi \pm nb)$, where $b = 0.35$ rad is the phase shift between the cases studied here and $n = \{1, 2, 3, 4\}$ for $\lambda = \{5.7, 2.8, 1.8, 1.4\}$.

To assess the usefulness of the effective reduced frequency, we consider the lift development of a VAWT-shaped motion at $k = 0.05$ and $\lambda = 1.4$, which is shown in figure 4 alongside the lift

Table 1. Effective reduced frequencies of the upstroke (k_{up}) and the downstroke (k_{down}) as a function of tip speed ratio λ and overall reduced frequency k.

λ	k	k_{up}	k_{down}	k	k_{up}	k_{down}
5.7	0.05	0.045	0.056	0.10	0.090	0.113
2.8	0.05	0.041	0.064	0.10	0.082	0.129
1.8	0.05	0.038	0.075	0.10	0.075	0.150
1.4	0.05	0.035	0.090	0.10	0.069	0.180

developments of sinusoidal motions at various reduced frequencies. The lift stall of the sinusoids shows a clear dependency on reduced frequency: the higher the reduced frequency, the higher the angle of attack at which the airfoil stalls. Figure 4a) reveals that stall at $k = 0.05$ and $\lambda = 1.4$ in fact occurs at the same time as stall of a sinusoid at $k = 0.02$, which is even lower than the effective reduced frequency of the upstroke $k_{up} = 0.035$. On the downstroke, shown in figure 4b), the stall of the VAWT-shape coincides with the stall of the sinusoid at $k = 0.10$, again more extreme than the effective reduced frequency of the downstroke $k_{down} = 0.090$. Despite these discrepancies, the sinusoids at the effective reduced frequencies of the upstroke and downstroke capture the angles of stall onset better than the sinusoid at the overall reduced frequency of $k = 0.05$.

The slower the upstroke, the deeper the stall, and the faster the downstroke, the later the reattachment. Therefore, the combination of slow upstroke and fast downstroke leads to a hysteresis in the lift coefficient at the beginning of the downstroke (cf. figure 4b) that is more severe than that of any sinusoidal motion. At the beginning of the upstroke (cf. figure 4a), the hysteresis is less severe because the combination of rapid downstroke and slow upstroke allows for less severe stall and faster reattachment.

4. Conclusions

The pressures and forces on an airfoil undergoing VAWT-shaped pitch motions corresponding to various tip speed ratios were compared to the those on a sinusoidally pitching airfoil in order to assess whether a sinusoidal motion represents a reasonable approximation of the motions of a VAWT blade. The lower the tip speed ratio, the larger the discrepancies between the sinusoidal motion and the VAWT-shaped motion. While the sinusoid appears to be a reasonable approximation of the motion at the highest tip speed ratios studied here, the motions at the lower tip speed ratios differed from the sinusoid in terms of the angles at which stall occurs, as well as the speed of reattachment on the downstroke. The dynamic stall angle can be captured reasonably well by instead considering a sinusoid at the effective reduced frequency of the half-cycle preceding the stall event. However, the delay in reattachment does not occur during sinusoidal motions at any reduced frequency.

This study has several short-comings. The surging of the freestream velocity experienced by a VAWT blade was neglected entirely, and its impact on the dynamic stall process is likely important. Furthermore, equation 3 assumes no interference from upstream blades and turbine tower. Studies on multi-bladed VAWTs show that the flow is in fact somewhat decelerated on the downstream half of the turbine [23], which leads to a very different flow field than the one considered here. However, this half of the turbine also produces very little thrust, so that inaccuracies in its modeling have less of an impact on overall performance predictions of VAWTs. Despite these shortcomings, sinusoidal motions provide significantly better approximations of the lift development of a VAWT-shaped pitching motion than static airfoil data and are likely

Table 2. Individual experimental runs in the pressurised High Reynolds number Test Facility at Princeton University. In all cases $\bar{\alpha} = 0°$ and $\hat{\alpha} = \pm 40°$.

Re_c	k	λ	P [MPa]	U_∞ [m/s]	f [Hz]	# of cycles
1.0×10^6	0.10	sine	11.57	0.86	0.160	148
1.0×10^6	0.10	5.7	11.54	0.85	0.161	148
1.0×10^6	0.10	2.8	11.64	0.85	0.159	148
1.0×10^6	0.10	1.8	11.66	0.84	0.159	148
1.0×10^6	0.10	1.4	11.76	0.84	0.156	148
1.0×10^6	0.05	sine	3.57	2.73	0.256	148
1.0×10^6	0.05	1.8	7.30	1.29	0.120	85
1.0×10^6	0.05	1.4	7.31	1.28	0.119	148
2.0×10^6	0.05	sine	11.56	1.71	0.160	148
2.0×10^6	0.05	5.7	10.60	1.86	0.174	148
2.0×10^6	0.05	2.8	12.54	1.60	0.150	148
2.0×10^6	0.05	1.8	15.64	1.38	0.128	148
2.0×10^6	0.05	1.4	12.42	1.62	0.151	148

to produce better agreement than existing dynamic stall corrections.

Acknowledgments
This work was funded by the United States National Science Foundation under grant CBET 1652583, and by the United States National Defense Science and Engineering Graduate Fellowship. The authors would like to thank Dan Hoffman at the Princeton Gas Dynamics Laboratory for his great help and advice in setting up the experiment, as well as Martin O. L. Hansen and an anonymous reviewer for helpful feedback.

Contributions
JK designed and built the airfoil setup. CEB conducted the experiments, analyzed the data and wrote the manuscript. All authors reviewed the paper. MH provided scientific advice and supervised the research.

Appendix
Cf. table 2

References
[1] Griffith D T, Barone M, Paquette J, Owens B, Bull D, Simao Ferreira C, Goupee A and Fowler M 2018 Design studies for deep-water floating offshore vertical axis wind turbines *Sandia National Laboratories Report*
[2] Brunner C E, Kiefer J, Hansen M O L and Hultmark M 2020 Unsteady effects on a pitching airfoil at conditions relevant for large vertical axis wind turbines *J. Phys.: Conf. Series* **1618** 052065
[3] Buchner A J, Soria J, Honnery D and Smits A J 2018 Dynamic stall in vertical axis wind turbines: scaling and topological considerations *J. Fluid Mech.* **841** 746–66
[4] Angulo I A and Ansell P J 2019 Influence of Aspect Ratio on Dynamic Stall of a Finite Wing *AIAA J.* **57** 7:2722-33
[5] Simao Ferreira C, Aagaard Madsen H, Barone M, Roscher B, Deglaire P and Arduin I 2014 Comparison of aerodynamic models for vertical axis wind turbines *J. Phys.: Conf. Series* **524** 012125

[6] Theodorsen T 1935 General theory of aerodynamic instability and the mechanism of flutter *NACA Tech. Report 496* 413–33
[7] Greenberg J M 1947 Airfoil in sinusoidal motion in a pulsating stream *NACA* TN-1326
[8] McCroskey W J 1981 The phenomenon of dynamic stall *NASA Tech. Memorandum 81264*
[9] Kiefer J, Brunner C E, Hansen M O L and Hultmark M Dynamic stall at high Reynolds numbers induced by ramp-type pitching motions *J. Fluid Mech.* **938** A10
[10] Dabiri J O, Greer J R, Koseff J R, Moin P and Peng J 2015 A new approach to wind energy: opportunities and challenges *AIP Conf. Proc.* **1652** 51
[11] Ayati A A, Steiros K, Miller M A, Duvvuri S and Hultmark M 2019 A double-multiple streamtube model for vertical axis wind turbines of arbitrary rotor loading *Wind Energ. Sci.* **4** 653–62
[12] Hezaveh S, Bou-Zeid E, Lohry M W and Martinelli L 2017 Simulation and wake analysis of a single vertical axis wind turbine *Wind Energ.* **20** 713–30
[13] Leishmann J G and Beddoes T S 1989 A Semi-Empirical Model for Dynamic Stall *J. Am. Helicopter Soc.* **34** 3:3–17
[14] Paraschivoiu I and Allet A 1988 Aerodynamic analysis of the darrieus wind turbines including dynamic-stall effects *J. Propuls. Power* **4** 5:472–7
[15] Dunne R and McKeon B J 2014 Dynamic separation on a pitching and surging airfoil as a model for flow over vertical axis wind turbine blades *32nd AIAA Applied Aerodynamics Conference*
[16] Wang S, Ingham D B, Ma L, Pourkashanian M and Tao Z 2010 Numerical investigations on dynamic stall of low Reynolds number flow around oscillating airfoils *Comput. Fluids* **39** 1529–41
[17] Simao Ferreira C, van Kuik G, van Bussel G and Scarano F 2009 Visualization by PIV of dynamic stall on a vertical axis wind turbine *Exp. Fluids* **46** 97–108
[18] Tsai H-C and Colonius T 2016 Coriolis effect on dynamic stall in a vertical axis wind turbine *AIAA J.* **54** 1:216–26
[19] Migliore P G, Wolfe W P and Fanucci J B 1980 Flow curvature effects on Darrieus turbine blade aerodynamics *J. Energy* **4** 2:49–55
[20] Miller M A, Duvvuri S, Brownstein I, Lee M, Dabiri J O and Hultmark M 2018 Vertical-axis wind turbine experiments at full dynamic similarity *J. Fluid Mech.* **844** 707–20
[21] Brunner C E, Kiefer J, Hansen M O L and Hultmark M 2021 Study of Reynolds number effects on the aerodynamics of a moderately thick airfoil using a high-pressure wind tunnel *Exp. Fluids* **62** 178
[22] Kiefer J, Brunner C E, Hultmark M and Hansen M O L 2020 Dynamic stall at high Reynolds numbers due to variant types of airfoil motion *J. Phys.: Conf. Series* **1618** 052028
[23] Parker C M and Leftwich M C 2016 The effect of tip speed ratio on a vertical axis wind turbine at high Reynolds numbers *Exp. Fluids* **57** 74